Title

Investigation of the Electronic Structure of Mono(1,1′-Diamidoferrocene) Uranium(IV) Complexes

Journal

Organometallics, 32(20)

ISSN

0276-7333

Authors

Duhović, Selma
Oria, Jeremy V
Odoh, Samuel O
et al.

Publication Date

2013-10-28

DOI

10.1021/om400521k

Peer reviewed

Investigation of the Electronic Structure of Mono(1,1'-Diamidoferrocene) Uranium(IV) Complexes

Selma Duhović,[a] Jeremy V. Oria,[a] Samuel O. Odoh,[b] Georg Schreckenbach,[b] Enrique R. Batista,[c] and Paula L. Diaconescu[a,*]

[a] Department of Chemistry and Biochemistry, University of California, Los Angeles, 607 Charles E Young Drive East, Los Angeles, CA 90095

[b] Department of Chemistry, University of Manitoba, Winnipeg, MB, Canada R3T 2N2

[c] Los Alamos National Laboratory, New Mexico, 87545

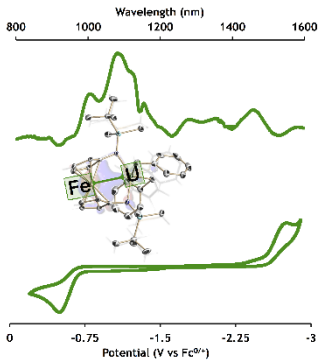

Supporting Information Placeholder

ABSTRACT: The electronic structure of several mono(1,1'-diamidoferrocene) uranium complexes (NN^{R})UX_2 (NN^{R} = $fc(NR)_2$, fc = 1,1'-ferrocenediyl, R = $SiMe_3$, Si^tBuMe_2, $SiMe_2Ph$, X = I, CH_2Ph), (NN^{TBS})UI(OAr) (OAr = 2,6-di-tert-butylphenoxide), and (NN^{TBS})U(CH_2Ph)(OAr) was investigated by electrochemistry, electronic absorption and vibrational spectroscopy, and DFT calculations. Similar metrical parameters were observed for (NN^{TBS})U(CH_2Ph)$_2$ and (NN^{DMP})U(CH_2Ph)$_2$ (and also for the previously reported (NN^{TMS})UI_2(THF), (NN^{TBS})UI_2(THF), and (NN^{TBS})U(CH_2Ph)(OAr)) that translate in similar DFT parameters (bond orders, metal charges) despite some small differences observed by electrochemistry and IR or electronic absorption spectroscopy.

1. INTRODUCTION

Our understanding of the importance of ancillary ligands in organometallic chemistry becomes increasingly sophisticated with the advance of characterization techniques. At one extreme, there are ligands such as phosphines and cyclopentadienyl derivatives that, once coordinated to the metal center, impart certain electronic and steric properties but are not modified during the course of a chemical transformation. At the other extreme, there are ligands that cooperate with the metal during its reactions.[1-3] The distinction between these two classes is becoming blurry[4] as tools that can reveal changes in the electronic and geometric structure of a metal complex during the course of a reaction become available.[5] However, dynamic studies of the reactivity of metal complexes are still in the realm of specialized techniques and most information is gathered by investigating metal complexes in the absence of substrates.

Our group has been interested in understanding the synergistic effects resulting from the interaction of ferrocene-based ligands with metals that exist in various oxidation states.[6-14] We have shown that such ligands are capable of influencing bonding and enhancing reactivity of transition metals,[8-11] lanthanides,[14-16] as well as actinides.[17-19] For uranium, we have observed a wide range of reactivity between tetravalent uranium complexes supported by such ligands and heterocycles.[20-23] For example, (NN^{TBS})U(CH_2Ph)$_2$ (NN^{TBS} = $fc(NSi^tBuMe_2)_2$, fc = 1,1'-ferrocenediyl) was found to mediate the double C-H activation, C-C coupling, alkyl transfer, and ring opening of aromatic N-heterocycles (Scheme 1). Some of these reactions were identified as separate steps, others as part of cascades.

The ferrocene backbone may have a specific role in facilitating the unique reactivity observed described above. When the electron rich iron center of ferrocene and the electropositive metal ion are brought into close proximity, a donor-acceptor interaction may take place between iron and the metal ion.[24] This type of Lewis acid-Lewis base interaction was observed previously with both electrophilic early and late transition metals.[25-29] Recently, our group reported a dative Fe-Ru interaction in $[Fe(\eta^5\text{-}C_5H_4NH)_2]Ru(PPh_3)_2$ and

characterized it by spectroscopic methods and DFT calculations.[30]

Scheme 1. Reactions of aromatic N-heterocycles mediated by $(NN^{TBS})U(CH_2Ph)_2$.

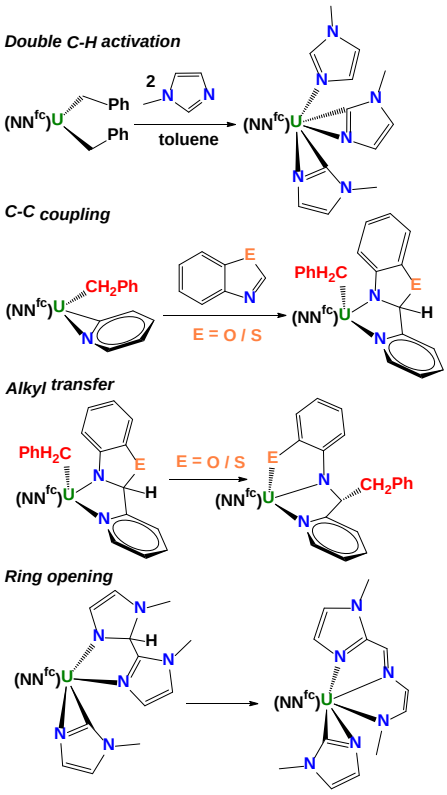

Of the examples reported, the Arnold group was the first to observe that the Fe-Ti distance in a series of compounds with the same NN^{TMS} (NN^{TMS} = fc($NSiMe_3$)$_2$) ligand varied according to the electrophilicity of the titanium center: the Fe-Ti distance is 3.32 Å in the neutral dialkyl complex $(NN^{TMS})TiMe_2$, but it shortens to 3.07 Å in the Lewis acid adduct $[(NN^{TMS})TiMe][MeB(C_6F_5)_3]$, and reaches the shortest value, at 2.49 Å, in the chloride bridging dicationic complex $([(NN^{TMS})Ti(\mu\text{-}Cl)]_2)[B(C_6F_5)_4]_2$. Our group observed a similar trend for group 3 metal complexes supported by the NN^{TBS} ligand: the Fe-Sc distance is 3.16 and 2.80 Å in $(NN^{TBS})Sc(CH_2C_6H_3Me_2\text{-}3,5)(THF)$ and $[(NN^{TBS})Sc(\mu\text{-}Cl)]_2$, respectively.[28] A similar Fe-M distance shortening was observed upon one electron oxidation of $(NN^{TBS})_2U$.[29] These examples show that the iron-metal interaction depends on the presence of other ligands coordinated to the metal center and becomes stronger when its electrophilicity increases.

In order to determine the role of the ferrocene backbone, we decided to initiate an in-depth investigation of the electronic structure of $(NN^{TBS})U(CH_2Ph)_2$. We approached this study by systematically analyzing the properties of several mono(1,1'-diamidoferrocene) uranium complexes using cyclic voltammetry, electronic absorption and vibrational spectroscopy, as well as computational methods. In addition to studies aimed at characterizing the iron-uranium interaction in $(NN^{TBS})U(CH_2Ph)_2$, the electronic properties of NN^{TBS} were compared to those of the ubiquitous Cp* (C_5Me_5) ligand.

2. RESULTS AND DISCUSSION

The following three uranium dibenzyl complexes (Chart 1) were compared: $(NN^{TMS})U(CH_2Ph)_2$, $(NN^{TBS})U(CH_2Ph)_2$, and $(NN^{DMP})U(CH_2Ph)_2$ (NN^{DMP} = fc($NSiMe_2Ph$)$_2$) in order to determine the role of the amide substituent. Although such modifications are minor, the NN^{TBS} ligand has a privileged role in our uranium studies and we were interested in determining whether a large difference exists between the electronic structures of the three complexes. In addition, in order to understand whether the ferrocene backbone interacts with uranium, we decided to compare $(NN^{TBS})U(CH_2Ph)_2$ with complexes in which the benzyl groups are replaced with other anionic ligands (Chart 1). This series consists of the following complexes: $(NN^{TBS})UI_2(THF)$, $(NN^{TBS})UI(OAr)$ (OAr = 2,6-di-*tert*-butylphenoxide), $(NN^{TBS})U(CH_2Ph)(OAr)$, and $(NN^{TBS})U(NPh_2)_2$.

Chart 1. Series of 1,1'-diamidoferrocene uranium complexes.

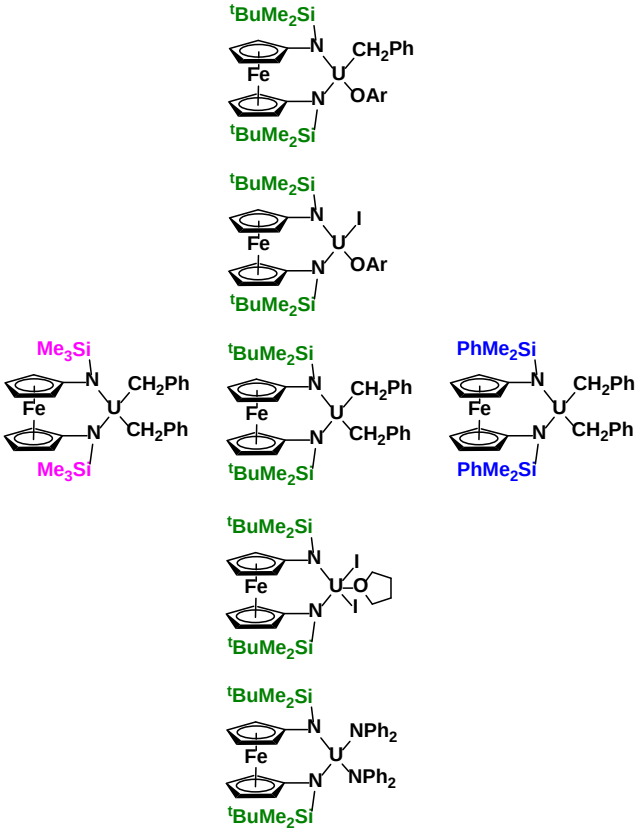

Solid-state Structural Characterization. Comparison of the metal-metal distances with the sum of covalent radii for the two metals has long been used to probe the presence of weak metal-metal interactions.[26, 31-36] Although the synthesis of $(NN^{TBS})U(CH_2Ph)_2$ was reported by us in 2008,[18] the data obtained from single-crystal X-ray diffraction was of low quality, preventing a detailed structural analysis. Since then,

collection of good quality data (Figure 1) allowed a redetermination of the crystal structure. In addition, $(NN^{DMP})U(CH_2Ph)_2$ was structurally characterized for the present study (Figure 1).

Both metal complexes feature a distorted tetrahedral environment around uranium if contacts with iron and the *ipso*-carbon atoms (ca. 2.8 Å) are ignored. The coordination of both benzyl ligands is η^2, and is more pronounced in $(NN^{TBS})U(CH_2Ph)_2$ (smaller UCC angles) than in $(NN^{DMP})U(CH_2Ph)_2$ (see Figure 1 caption for values). The most important feature for the present study, however, is the iron-uranium distance of 3.1878(5) Å in $(NN^{TBS})U(CH_2Ph)_2$ and 3.1874(4) Å in $(NN^{DMP})U(CH_2Ph)_2$. For comparison, the same distance is 3.2039(5) Å in $(NN^{TBS})U(CH_2Ph)(OAr)$,[37] 3.1786(24) Å in $(NN^{TBS})UI_2(THF)$, and 3.2323(5) Å in $(NN^{TMS})UI_2(THF)$;[19] all these distances are shorter than the sum of the iron and uranium covalent radii (3.28 Å).[38] Other structural parameters used to probe iron-metal interactions in ferrocene-based complexes are the Cp-ring twist angle and the Cp-Cp tilt angle (see Figure S44 for a description of these parameters). The Cp-ring twist angle is 3.6º in $(NN^{TBS})U(CH_2Ph)_2$ and 10.3º in $(NN^{DMP})U(CH_2Ph)_2$, while the Cp-Cp tilt angle is 121.2º in $(NN^{TBS})U(CH_2Ph)_2$ and 121.6º in $(NN^{DMP})U(CH_2Ph)_2$; for comparison, the Cp-Cp tilt angle in ferrocene is 107.4°. These values indicate an appreciable distortion of the ferrocene ligand as has been observed previously by us for metal complexes with weak iron-metal interactions.[9]

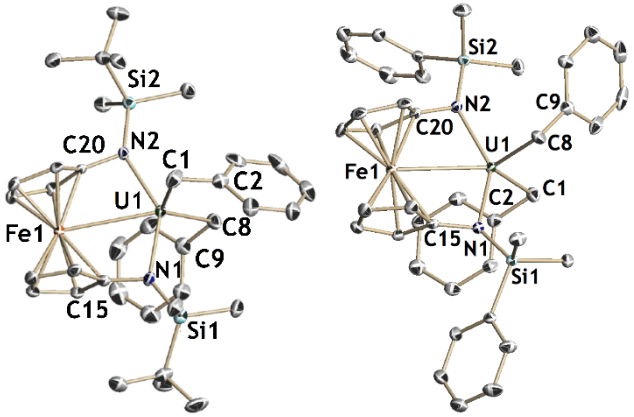

Figure 1. Thermal-ellipsoid (50% probability) representation of $(NN^{TBS})U(CH_2Ph)_2$ (left) and $(NN^{DMP})U(CH_2Ph)_2$ (right) with hydrogen atoms omitted for clarity. Selected distances [Å] and angles [°] for $(NN^{TBS})U(CH_2Ph)_2$: U(1)-Fe(1), 3.1878(05); U(1)-C(1), 2.5153(37); U(1)-C(8), 2.4827(36); U(1)-N(1), 2.2241(29); U(1)-N(2), 2.2295(27); U(1)-C(1)-C(2), 87.65(22); U(1)-C(8)-C(9), 92.96(21); N(2)-U(1)-N(1), 139.82(10); U(1)-N(1)-C(15), 100.83(20); U(1)-N(2)-C(20), 98.99(18); Fe(1)-C(15)-N(1), 128.55(23); Fe(1)-C(20)-N(2), 130.39(21); U(1)-N(2)-Si(2), 143.16(15); U(1)-N(1)-Si(1), 133.85(16); C(15)-Fe(1)-C(20), 121.21(13). Selected distances [Å] and angles [°] for $(NN^{DMP})U(CH_2Ph)_2$: U(1)-Fe(1), 3.1874(04); U(1)-C(1), 2.4781(21); U(1)-C(8), 2.4648(22); U(1)-N(1), 2.2249(16); U(1)-N(2), 2.2141(16); U(1)-C(1)-C(2), 91.58(12); U(1)-C(8)-C(9), 100.59(13); N(1)-U(1)-N(2), 139.08(06); U(1)-N(1)-C(15), 100.92(11); U(1)-N(2)-C(20), 100.28(11); Fe(1)-C(15)-N(1), 128.09(13); Fe(1)-C(20)-N(2), 128.98(13); U(1)-N(2)-Si(2), 141.12(09); U(1)-N(1)-Si(1), 131.82(09); C(15)-Fe(1)-C(20), 121.56(7).

Cyclic Voltammetry. Electrochemical measurements of uranium dibenzyl complexes supported by the different diamidoferrocene ligands were conducted in α,α,α-trifluorotoluene (TFT) and diethyl ether, separately, with $TPABAr^F$ ($[^iPr_4N][B(3,5\text{-}(CF_3)_2C_6H_3)_4]$) as the supporting electrolyte. Although tetravalent uranium alkyl complexes have been shown to activate carbon-fluorine bonds of perfluorocarbons,[39] we note that ^1H NMR spectra of all $(NN^R)U(CH_2Ph)_2$ complexes measured after the electrochemical experiments showed no decomposition. Attempts to carry out voltammetric experiments in other solvents capable of dissolving both the supporting electrolyte and the uranium dibenzyl complexes were unsuccessful. Specifically, the former is insoluble in toluene and hydrocarbons, while the latter decompose in solvents such as THF and CH_2Cl_2. Experiments conducted in diethyl ether exhibit anodic waves that could not be interpreted; the coordination ability of diethyl ether is the most likely culprit because similar voltammetric behavior is observed upon addition of THF during measurements in TFT (see Figures S8 and S9 for details).

As shown in Figure 2, when TFT was used as the solvent, $(NN^{TMS})U(CH_2Ph)_2$, $(NN^{TBS})U(CH_2Ph)_2$, and $(NN^{DMP})U(CH_2Ph)_2$ exhibit one reduction event between -2.7 V and -3.0 V; a small difference in reduction potentials is observed. Specifically, uranium is slightly more difficult to reduce when it is supported by NN^{TMS} (E_{red} = -2.94 V) than by NN^{TBS} (E_{red} = -2.75 V) and NN^{DMP} (E_{red} = -2.74 V). Although the differences between the three dibenzyl uranium complexes are small, the reduction potential for $(NN^{TBS})U(CH_2Ph)_2$, featuring the electron donating *t*-butyl group, is similar to that of $(NN^{DMP})U(CH_2Ph)_2$, which features the electron withdrawing phenyl group, and not to that of the TMS analogue ($(NN^{TMS})U(CH_2Ph)_2$), bearing the electron donating methyl group. Furthermore, it is apparent that no current is generated on the reverse scan, implying that products of those reductions are unstable on the measurement time scale and are consumed in a chemical reaction. Increasing the scan rate of the applied potential revealed no change in the overall wave shapes (Figure S4), suggesting that the half-lives of these follow-up reactions are considerably lower than the duration of the scan.[40-41] It is interesting to note that uranium is more difficult to reduce in $(NN^R)U(CH_2Ph)_2$ than when it is supported by pentamethylcyclopentadienyl ligands. For example, $(C_5Me_5)_2U(CH_2Ph)_2$ undergoes reduction at -1.95 V.[42] This increase in reduction potential implies that the electron density around uranium is greater when it is supported by 1,1'-diamidoferrocene than pentamethylcyclopentadienyl ligands.

The main anodic event (between -0.50 and -0.75 V) is attributed to the oxidation of the iron center, which is most difficult to oxidize in NN^{TBS} and least difficult in the NN^{TMS} analogue. Although there is no correlation between the oxidation potential of iron and the electronic nature of silylamido substituents, the trend correlates with the steric properties of the amide substituents. Specifically, the effective steric bulk, as well as steric interaction, of a substituent is

measured by A values, which follow the order *t*-Bu (A = 4.9) > Ph (A = 2.7) > Me (A = 1.8).[43] This trend, therefore, implies that the greater steric bulk of the *t*-butyl group on the amide substituent destabilizes the oxidized state of iron with respect to the methyl and phenyl analogues.

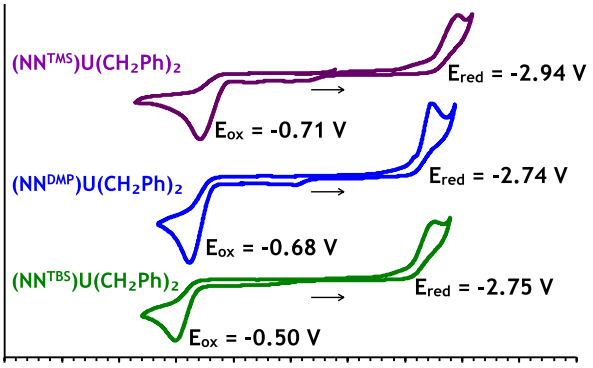

Figure 2. Cyclic voltammograms of $(NN^{R})U(CH_2Ph)_2$ at a scan rate of 100 mV/s in TFT with $TPABAr^{F}$ as the supporting electrolyte.

It is worth noting that the overall electrochemical profiles of $(NN^{R})U(CH_2Ph)_2$ complexes are dependent on both the direction and the magnitude of maximum applied potential (Figure 3). For example, the main oxidation event in $(NN^{TMS})U(CH_2Ph)_2$ occurs at approximately -0.71 V (wave A in Figure 3) when the scan is performed oxidatively. Two reductive events at -2.03 V and -2.36 V are also observed (A' and B in Figure 3). The former is attributed to the reduction of the species formed upon oxidation (represented by wave A), while the latter is likely due to reduction of 1,2-diphenylethane (Figure 3). Comparison of the electrochemical profile of $(NN^{TMS})U(CH_2Ph)_2$ with that of 1,2-diphenylethane, whose cyclic voltammogram was collected by us under the same conditions (Figure 3), shows that the benzyl radical undergoes radical-radical coupling. Consequently, this allows us to attribute the anodic event at -2.32 V (wave B' in Figure 3) to 1,2-diphenylethane. Reduction of 1,2-diphenylethane can generate a radical anion, which can undergo dimerization, disproportionation, fragmentation, or protonation.[44] Regardless of its fate, formation of 1,2-diphenylethane indicates that oxidation of 1,1'-diamidoferrocene uranium dibenzyl complexes proceeds via a radical mechanism.

Exact assignment of the inherently irreversible oxidative event observed at -1.68 V (wave C' in Figure 3) when the scan was performed in the reductive direction, however, is more difficult. It is clearly due to an electroactive species formed as a result of the main reductive event at -2.99 V (wave C in Figure 3), but the identity of these species is unknown. Comprehensive measurements can be found in Figure S7 of the Supporting Information.Next, we investigated the electrochemical behavior of complexes with the same ferrocene backbone (NN^{TBS}) and varied the labile ligands (CH_2Ph, I, ArO, Ph_2N). As shown in Figure 4, replacing one benzyl ligand with an aryloxide increases the oxidation potential of iron by 240 mV (E_{ox} = -0.50 V in $(NN^{TBS})U(CH_2Ph)_2$ vs. -0.26 V in $(NN^{TBS})U(CH_2Ph)(OAr)$). Replacing benzyl with diphenylamide ligands has the same effect (E_{ox} = -0.19 V). This trend, i.e. more electron donating ligands destabilize the oxidized states for both metals instead of stabilizing them, is unexpected and difficult to explain. As discussed below, DFT calculations show similar parameters for the iron-uranium interaction in the $(NN^{R})U(CH_2Ph)_2$ and $(NN^{R})UI_2(THF)$ series, indicating that other factors may determine the changes observed by cyclic voltammetry.

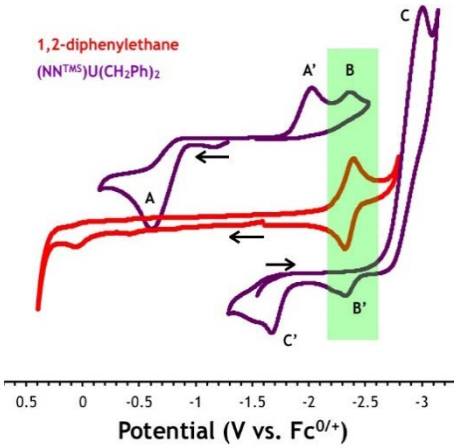

Figure 3. Cyclic voltammograms of $(NN^{TMS})U(CH_2Ph)_2$ and 1,2-diphenylethane. Both studies were conducted in TFT with $TPABAr^{F}$ as the supporting electrolyte and a scan rate of 10 mV/s.

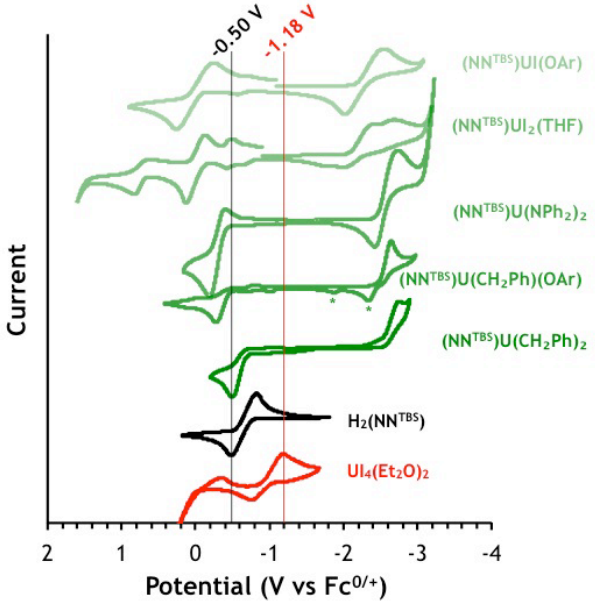

Figure 4. Cyclic voltammograms of $(NN^{TBS})UX_2$ complexes. All measurements were performed in THF with $TPABAr^{F}$ as the supporting electrolyte, except for $(NN^{TBS})U(CH_2Ph)_2$, in which case the solvent used was TFT. Cyclic voltammograms of $UI_4(Et_2O)_2$ and $H_2(NN^{TBS})$ were measured in Et_2O and CH_2Cl_2, respectively. Black and red vertical lines at -0.50 and -1.18 V represent the oxidation of iron and reduction of uranium in $H_2(NN^{TBS})$ and $UI_4(Et_2O)_2$, respectively.

When both benzyl ligands are replaced by iodides, the anodic profile becomes more complicated: the main oxidation wave shifts to even more positive potentials (E_{ox} = 0.13 V), while an additional anodic event observed at 0.80 V is ascribed to oxidation of uranium. Our reasoning for this assignment is based on the observation that the electron donating ability of diamidoferrocene ligands is strong enough to destabilize the trivalent state of uranium (i.e. shift the *reduction* potential to more negative values compared to the $UI_4(Et_2O)_2$ precursor, Figure 4) and at the same time, stabilize its pentavalent state (i.e. shift the *oxidation* potential to more negative values). Finally, oxidation of iron is most difficult with the introduction of mixed ligands. Specifically, the oxidation potential of $(NN^{TBS})UI(OAr)$ is greater than that of $(NN^{TBS})U(CH_2Ph)_2$ by almost 800 mV.

The reduction potential of uranium, which is irreversible in $(NN^{R})U(CH_2Ph)_2$ complexes, is essentially constant upon replacement of one benzyl with an aryloxide ligand (E_{red} = -2.72 V in $(NN^{TBS})U(CH_2Ph)_2$ versus -2.63 V in $(NN^{TBS})U(CH_2Ph)(OAr)$). As shown in Figure 4, the reduction of $(NN^{TBS})U(CH_2Ph)(OAr)$ is followed by a chemical transformation of the reduction product to an unknown redox active species (marked by asterisks in Figure 4). In contrast, the reduction of uranium in $(NN^{TBS})U(NPh_2)_2$ (E_{red} = -2.69 V) becomes more reversible. Moreover, as expected, introducing iodide ligands decreases the reduction potential, as exemplified by the electrochemical profiles of $(NN^{TBS})UI_2(THF)$ and **(**NN^{TBS})UI(OAr) complexes (E_{red} = -2.35 V and -2.55 V, respectively).

Near-Infrared Spectroscopic Studies. For uranium complexes, intraconfigurational f→f transitions are Laporte forbidden and appear as weak bands in the near infrared (NIR) region.[45-48] Spectral features arising from these transitions are expected to remain roughly constant upon changing the ligand environment around the uranium center.

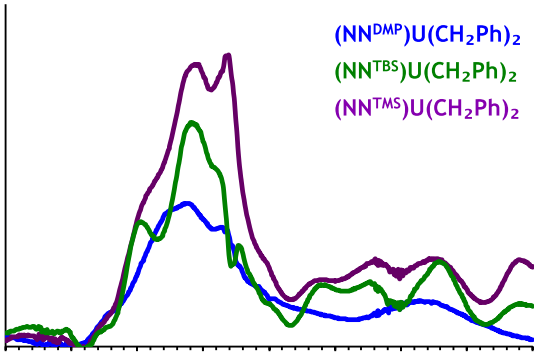

Figure 5. NIR spectra of $(NN^{R})U(CH_2Ph)_2$ complexes (16-23 mM in toluene).

As shown in Figure 5, NIR spectra of 1,1'-diamidoferrocene uranium dibenzyl complexes are characterized by absorption bands of low intensity (ε = 20–80 $M^{-1}cm^{-1}$), with a broad band centered at approximately 1080 nm. The nearly identical features across this series suggest that these bands likely arise from electronic transitions within the uranium core. It is interesting to note that, in late transition metal complexes supported by chelating ferrocene ligands,[9] short iron-metal distances are associated with metal-to-metal charge transfer bands in the NIR region with intensities of the order of 10^2 $M^{-1}cm^{-1}$. Those bands allowed further characterization of the iron-metal interaction by resonance Raman spectroscopy. The lack of such metal-to-metal charge transfer bands for the uranium complexes studied here indicates that the iron-uranium interaction is weaker or less covalent than in corresponding late transition metal complexes, an interpretation supported by the results of DFT calculations (see below).

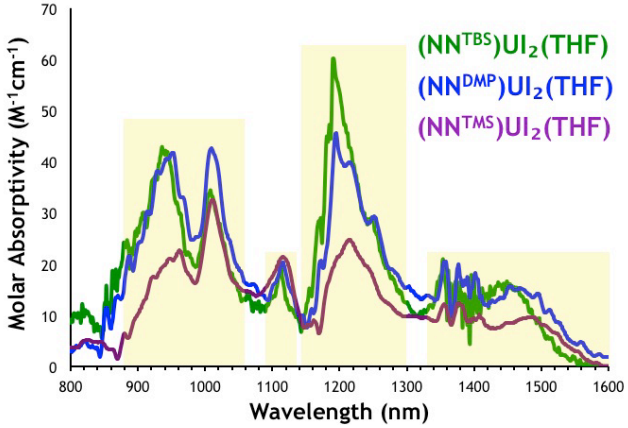

Figure 6. NIR spectra of $(NN^{R})UI_2(THF)$ complexes (9-19 mM in THF).

The NIR spectra of $(NN^{R})UI_2(THF)$ complexes supported by different silylamido ferrocene backbones are also nearly identical (Figure 6). All spectra feature five bands centered at approximately 950 nm, 1020 nm, 1150 nm, 1230 nm, and 1450 nm, with molar absorptivity values characteristic of f→f transitions within the uranium core. Like for $(NN^{R})U(CH_2Ph)_2$ complexes, these bands are positioned at the same energies, suggesting that the three $(NN^{R})UI_2(THF)$ compounds have similar electronic structures.

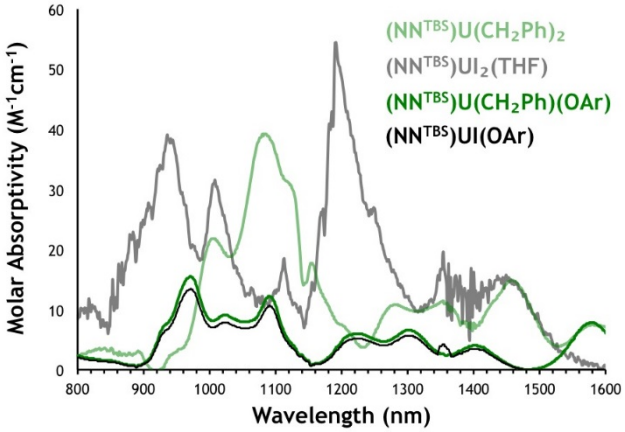

Figure 7. NIR spectra of $(NN^{TBS})UX_2$ complexes; $(NN^{TBS})UI(OAr)$ (17.9 mM in toluene), $(NN^{TBS})UI_2(THF)$ (9.3 mM in THF), $(NN^{TBS})U(CH_2Ph)_2$ (23.5 mM in toluene), $(NN^{TBS})U(CH_2Ph)(OAr)$ (23.1 mM in toluene).

A comparison between the NIR spectral profiles of the $(NN^{TBS})UX_2$ series shows differences between these spectra (Figure 7) that indicate that the electronic structure of the uranium core is somewhat perturbed by the labile ligands (CH_2Ph, I, ArO, Ph_2N). We draw attention to the similarity between the NIR spectra of complexes bearing mixed labile ligands, i.e. $(NN^{TBS})UI(OAr)$ and $(NN^{TBS})U(CH_2Ph)(OAr)$, both of which have different spectra than those for complexes of homologous ligands, i.e. $(NN^{TBS})UI_2(THF)$ and $(NN^{TBS})U(CH_2Ph)_2$.

UV-Vis Spectroscopic Studies. Spectra of organoactinide complexes show, in the UV-Vis region, interconfigurational f→d transitions,which are allowed and thus give rise to intense absorption bands at high energy,[49] and absorption bands originating from charge transfer between the actinide and its ligands. Like f→d transitions, charge transfer bands are observed at high energy but are typically more intense.[50-53] Moreover, the energy of charge transfer bands is affected by both the nature of the ligand and the oxidation state of the metal, as well as the distance between them.[49] In addition, absorption bands for the compounds discussed herein may also originate from electronic transitions based on the iron center, as well as their interaction with amido substituents or uranium.

As shown in Figure 8, an absorption band at approximately 400 nm is observed in the UV-Vis spectra of $(NN^{R})UI_2(THF)$ complexes. The large extinction coefficient values (1100-1900 $M^{-1}cm^{-1}$) preclude d→d transitions within the iron center as its origin. Charge transfer between the two metal centers can also be ruled out because the energy of the transition is too high across the series. Based on previously reported electronic absorption spectra of tetravalent uranium complexes,[54-61] it is likely that this band arises from a combination of 5f→6d transitions within the uranium core and iodide→uranium charge transfer. This assignment is further supported by the observed similarity between the voltammograms (Figure 4) and absorption spectra of $(NN^{TBS})UI_2(THF)$ and $(NN^{TBS})UI(OAr)$, as well as the absence of such an intense band in $(NN^{TBS})U(CH_2Ph)_2$, $(NN^{TBS})U(CH_2Ph)(OAr)$, and $(NN^{TBS})U(NPh_2)_2$ (Figure 9).

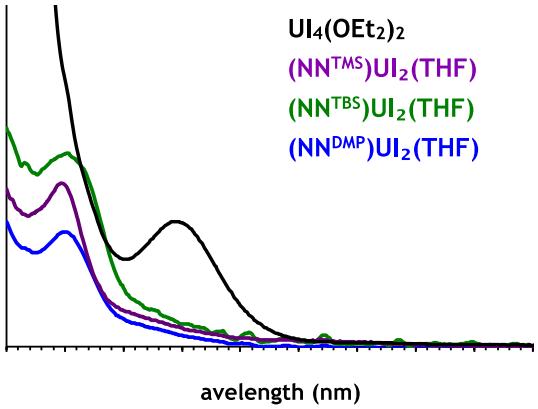

Figure 8. UV-Vis spectra of $(NN^{R})UI_2(THF)$ complexes (0.3-0.5 mM in THF) and $UI_4(Et_2O)_2$ (0.7 mM in Et_2O).

UV-Vis spectra of all three uranium dibenzyl complexes (Figure 10) are also nearly identical, featuring a strong absorption band (10^3 $M^{-1}cm^{-1}$) at approximately 300 nm, and a lower intensity band (10^2 $M^{-1}cm^{-1}$) around 425 nm. Based on the discussion above for the corresponding diiodide uranium complexes, the first band is assigned to 5f→6d transitions within the uranium core, while the latter is assigned to d→d transitions within ferrocene. The assignment of the latter band is supported by the presence of a similar absorption in the UV-Vis spectrum of $H_2(NN^{TBS})$ (Figure 9). Unfortunately, overall, the electronic absorption spectra of complexes investigated herein do not provide any specific information that can be related to the iron-uranium interaction.

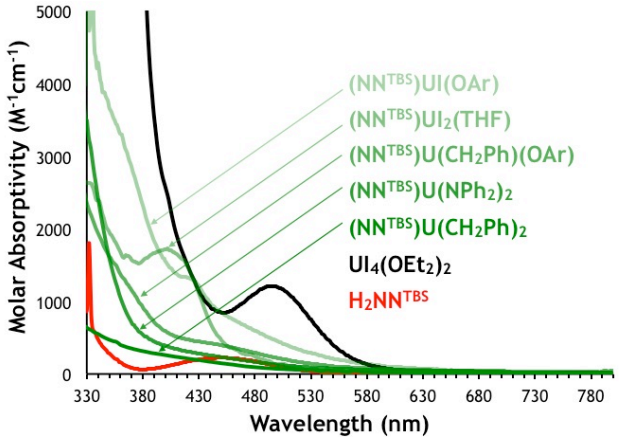

Figure 9. UV-Vis spectra of $(NN^{TBS})UX_2$ complexes; $UI_4(Et_2O)_2$ precursor (0.7 mM in Et_2O), H_2NN^{TBS} (2.8 mM in CH_2Cl_2), $(NN^{TBS})UI(OAr)$ (0.5 mM in THF), $(NN^{TBS})UI_2(THF)$ (0.4 mM in THF), $(NN^{TBS})U(CH_2Ph)_2$ (0.1 mM in toluene), $(NN^{TBS})U(CH_2Ph)(OAr)$ (0.25 mM in toluene), $(NN^{TBS})U(NPh_2)_2$ (0.21 mM in toluene).

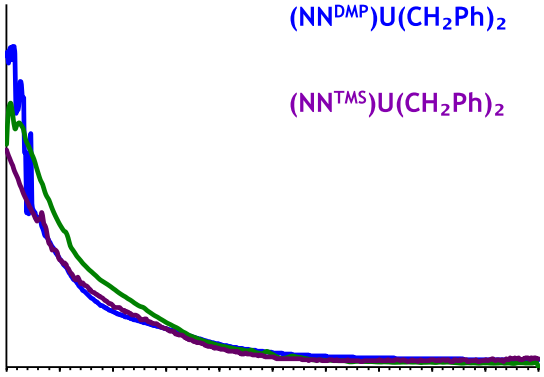

Figure 10. UV-Vis spectra of $(NN^{R})U(CH_2Ph)_2$ complexes (1-4 mM in toluene).

Vibrational Spectroscopy. In order to gain further insight into the electronic structures of 1,1'-diamidoferrocene uranium complexes, we analyzed the infrared spectra of dibenzyl and diiodide derivatives. As shown in Figure 11, the IR spectra of $(NN^{R})U(CH_2Ph)_2$ complexes are similar. The phenyl-bearing silylamido analogue ($(NN^{DMP})U(CH_2Ph)_2$), however, features one extra band at 1131 cm^{-1}, which likely corresponds to the C-

C stretch of the phenyl rings since they are absent in $(NN^{TMS})U(CH_2Ph)_2$ and $(NN^{TBS})U(CH_2Ph)_2$.

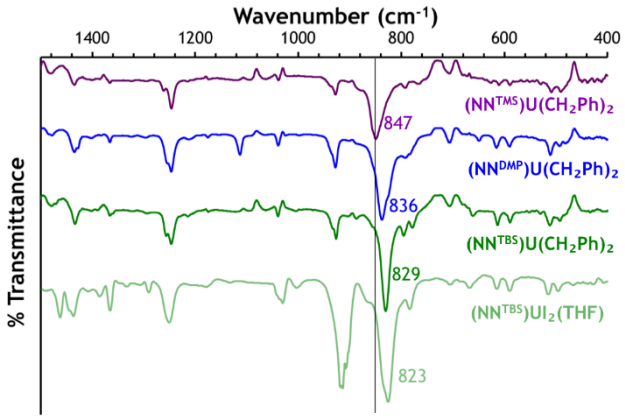

Figure 11. IR spectra of $(NN^R)U(CH_2Ph)_2$ and $(NN^{TBS})UI_2(THF)$ in toluene and THF, respectively.

Previous studies on ferrocene and ferrocenium derivatives have found that the energy of the perpendicular C-H bending on both Cp rings is sensitive to changes in the electron density at the iron center and that the band corresponding to this vibrational mode shifts to *higher* energy upon oxidation of ferrocene (805 cm^{-1} in ferrocene vs. 851 cm^{-1} in ferrocenium).[62] Upon closer inspection, it becomes clear that, unlike all others, the most prominent band in the IR spectra shifts depending on the substituents of the ferrocene backbone. For example, in the $SiMe_3$ analogue ($(NN^{TMS})U(CH_2Ph)_2$), this band is centered at 847 cm^{-1} but shifts to 836 cm^{-1} when a phenyl ring replaces one methyl group ($(NN^{DMP})U(CH_2Ph)_2$). The *t*-butyl group in $(NN^{TBS})U(CH_2Ph)_2$ instead further shifts the band to 829 cm^{-1}. In addition, the IR spectrum of $(NN^{TBS})UI_2(THF)$ (Figure 12) is essentially identical to that of $(NN^{TBS})U(CH_2Ph)_2$. According to DFT calculations for $(NN^R)UI_2(THF)$ and $(NN^R)U(CH_2Ph)_2$, this strong band corresponds to vibrational modes involving C-H bonds of the methyl groups on silylamido substituents. This stretching mode results in no change in the metal-metal distance. Therefore, this downward shift in energy (Me > Ph > ^{t}Bu) is likely a consequence of steric rather than electronic factors.

DFT Calculations. The coordinates for $(NN^R)U(CH_2Ph)_2$, $(NN^R)UI_2(THF)$ (R = TMS, TBS, DMP), and $(NN^{TBS})U(CH_2Ph)(OAr)$ were optimized using ADF2012.01.[63-64] An f^2 electronic configuration was assumed for all ground states based on experimental results (i.e. calculations were carried out using the spin unrestricted formalism with two α spins in excess of β spins). The value for the calculated Fe-U distance in $(NN^{TBS})U(CH_2Ph)_2$, 3.21 Å (see Table S1 in the Supporting Information for other parameters and other compounds), matches well the experimental distance determined by X-ray crystallography (3.19 Å, see above). Mulliken and Hirshfeld charges have been employed previously by us to characterize weak metal-metal interactions.[7, 9] Our results indicate that while the Mulliken charges do not differ between the three $(NN^R)U(CH_2Ph)_2$ complexes, the Hirshfeld charge is somewhat higher for uranium in $(NN^{TMS})U(CH_2Ph)_2$ (Table 1). In addition, the energies of the frontier molecular orbitals (Figure 12) show similarities between the three complexes, with a slight difference between $(NN^{TMS})U(CH_2Ph)_2$ and $(NN^{TBS})U(CH_2Ph)_2$, on one hand, and $(NN^{DMP})U(CH_2Ph)_2$ on the other. These results support our experimental findings, which show that the differences between the electronic structures of the three uranium dibenzyl complexes are small.

Table 1. Calculated parameters for $(NN^R)U(CH_2Ph)_2$.

		NN^{TMS}	NN^{TBS}	NN^{DMP}
Mulliken Charges	U	2.48	2.46	2.44
	Fe	0.40	0.43	0.38
Hirshfeld Charges	U	0.76	0.68	0.67
	Fe	0.06	0.06	0.06
Natural Charge	U	1.49	1.47	1.50
	Fe	0.13	0.12	0.12
Net Overlap	Fe-U	0.07	0.07	0.07
Natural Bond Order	Fe-U	0.03	0.03	0.03

The Mayer bond orders for the Fe–U interaction in $(NN^{TMS})U(CH_2Ph)_2$, $(NN^{TBS})U(CH_2Ph)_2$, and $(NN^{DMP})U(CH_2Ph)_2$ were calculated at 0.38, 0.39, and 0.41, respectively. For comparison, the bond order for the Fe-Ru interaction in $[fc(NH)_2]Ru(PPh_3)_2$ was found to be 0.26.[9] While the increased Lewis acidity of uranium compared to that of ruthenium might account for the higher calculated bond order, it is important to mention that the average Mayer bond orders for U-N and U-C interactions in $(NN^{TBS})U(CH_2Ph)_2$ are 0.73 and 0.37, respectively. The diiodide complexes were found to have similar Mayer bond orders: $(NN^{TMS})UI_2(THF)$ (0.32), $(NN^{TBS})UI_2(THF)$ (0.35), and $(NN^{DMP})UI_2(THF)$ (0.32). It is important to note that Nalewajski-Mrozek bond orders (calculated from two-electron valence indices, 3-index set) have been recognized to describe binding with a strong ionic component better than Mayer values.[65-66] For comparison, the Nalewajski-Mrozek bond order for the Fe-U interaction and averages for the U-N and U-C bond orders in $(NN^{TBS})U(CH_2Ph)_2$ are 0.71, 1.32, and 0.91, respectively (see Tables S10-S16 for other values). These values indicate that while the iron-metal interactions are weaker than single bonds, electron donation from iron to uranium likely takes place.

Natural bond order analysis[67] also showed similarities between the three $(NN^R)U(CH_2Ph)_2$ complexes (Table 1). The net overlap between iron and uranium as well as natural bond orders for Fe-U have the same value in all $(NN^R)U(CH_2Ph)_2$ complexes. $(NN^{DMP})U(CH_2Ph)_2$ and $(NN^{TBS})U(CH_2Ph)_2$ bear two iron-centered (>70%) natural localized molecular orbitals (NLMOs) that have uranium contributions greater than 5%. Considering that uranium carries a more positive charge than iron, the calculated NLMOs (Figures S52-S54) indicate that there is electron donation from iron to uranium. Moreover, frontier molecular orbitals agree with this depiction: two molecular orbitals for $(NN^{TBS})U(CH_2Ph)_2$ (HOMO-3 and HOMO-7, Figure 13) and $(NN^{DMP})U(CH_2Ph)_2$ (HOMO-5 and HOMO-6, Figure S56), and one for $(NN^{TMS})U(CH_2Ph)_2$ (HOMO-3, Figure S54) show overlap between iron and uranium atomic orbitals. Interestingly, although the uranium

contribution is small in all cases, the f orbitals are the main participants used for this interaction.

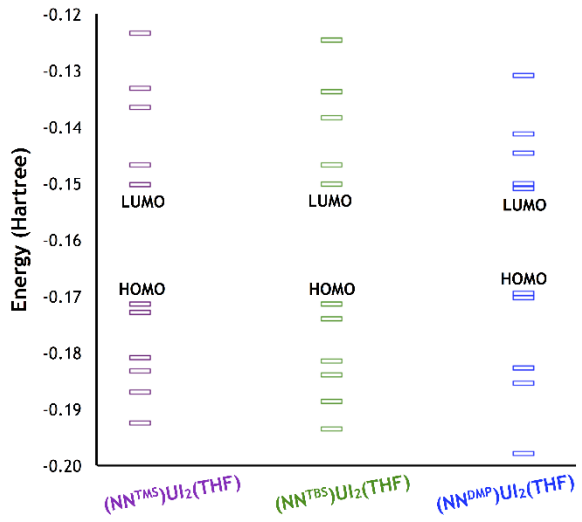

Figure 12. Partial MO diagrams of $(NN^{R})U(CH_2Ph)_2$.

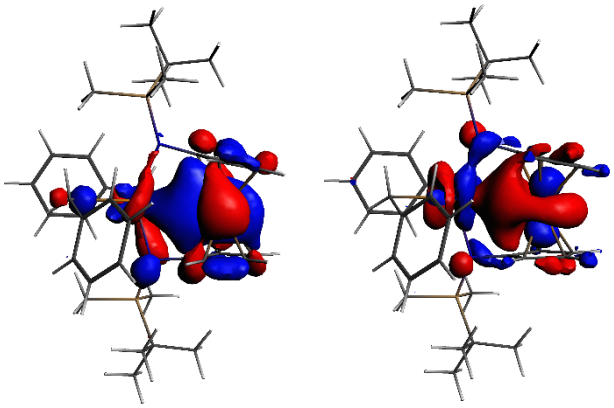

Figure 13. Molecular orbitals (isosurface value = 0.02) for $(NN^{TBS})U(CH_2Ph)_2$: HOMO-3 (left) and HOMO-7 (right).

Table 2. Calculated Bader parameters for $(NN^{R})U(CH_2Ph)_2$/$(NN^{R})UI_2(THF)$.

	NN^{TMS}	NN^{TBS}	NN^{DMP}
Bader Charge (U)	1.44/1.39	1.44/1.41	1.44/1.42
Bader Charge (Fe)	0.60/0.65	0.61/0.65	0.60/0.53
Fe-U ($\nabla^2\rho$)	0.017/0.022	0.024/0.021	0.015/0.025
Fe-U ρ	0.012/0.013	0.013/0.014	0.013/0.017

In order to characterize the iron-uranium interaction further, we employed Bader's Atoms in Molecules (AIM) theory.[68-69] Bader charges on uranium and iron are nearly identical in each case for $(NN^{R})U(CH_2Ph)_2$ and $(NN^{R})UI_2(THF)$ complexes (Table 2). More importantly, AIM has been used to characterize bonds between two metal centers[70] and in ferrocene complexes.[71] AIM identifies any type of bond by determining whether a (3, -1) critical point exists between two atoms. A (3, -1) critical point was located in each $(NN^{R})U(CH_2Ph)_2$ complex at 1.60 Å (Figure S52), which is the midpoint of the Fe-U distances, supporting the presence of a weak interaction between the two metal centers.

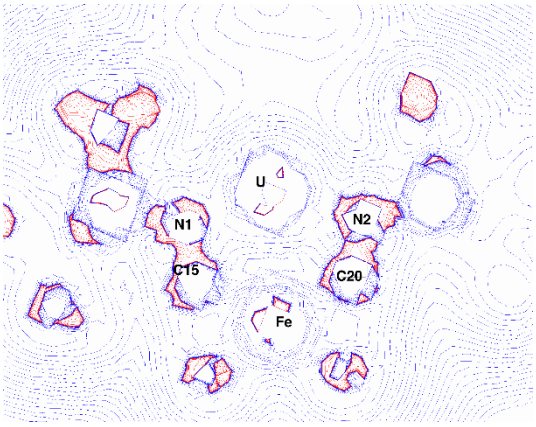

Figure 14. Contour plot of the Laplacian of charge density for $(NN^{TBS})U(CH_2Ph)_2$. Red lines indicate areas of high charge $\nabla^2\rho < 0$, blue lines indicate depletion of charge $\nabla^2\rho > 0$.

A distinction between covalent bonds from weak interactions (i.e. hydrogen bond, van der Waals, and donor-acceptor) can be made using the value of the Laplacian of charge density ($\nabla^2\rho$). Specifically, $\nabla^2\rho > 0$ corresponds to a weak interaction, while $\nabla^2\rho < 0$ indicates a covalent bond. In all $(NN^{R})U(CH_2Ph)_2$ complexes, the value of $\nabla^2\rho$ is greater than 0 (Table 2), suggesting the presence of a non-covalent interaction. Compound $(NN^{TBS})U(CH_2Ph)_2$, with the highest $\nabla^2\rho$ value, features the most ionic interaction between iron and uranium of the three dibenzyl complexes studied. In addition, the contour plot of the Laplacian of charge density for $(NN^{TBS})U(CH_2Ph)_2$ in the plane of iron, uranium, and one of the amide nitrogen atoms (Figure 14) shows low electron density between the two metal centers and a gradient that is consistent with a weak interaction. This is in contrast with the higher gradient observed between the amide nitrogen and carbon atoms (N1–C15 and N2–C20), which form a covalent bond.

3. CONCLUSIONS

We have systematically analyzed the properties of several mono(1,1'-diamidoferrocene) uranium complexes using cyclic voltammetry, electronic absorption and vibrational spectroscopy, as well as computational methods. Varying the amide substituents on the ferrocene backbone bestows little influence on the oxidation of iron and the reduction of uranium in the three $(NN^{TBS})U(CH_2Ph)_2$ complexes. However, the ferrocene diamides significantly increase the reduction potential of uranium, which suggests that they are stronger electron donors than pentamethylcyclopentadienyl ligands. Similar metrical parameters were observed for $(NN^{TBS})U(CH_2Ph)_2$ and $(NN^{DMP})U(CH_2Ph)_2$ (and also for the previously reported $(NN^{TMS})UI_2(THF)$, $(NN^{TBS})UI_2(THF)$, and $(NN^{TBS})U(CH_2Ph)(OAr)$) that translate in similar DFT parameters (bond orders, metal charges) despite some small differences observed by electrochemistry and vibrational or

electronic absorption spectroscopy. Overall, changes in ligands had a minor effect on the iron-uranium interaction and the usual characterization spectroscopic methods are not sensitive enough to measure them. DFT calculations provided additional information (natural bond order analysis and Bader's atom in molecules method) and is the only method that, together with X-ray crystallography, allowed the characterization of the iron-uranium bond as a weak donor-acceptor interaction in these complexes.

4. EXPERIMENTAL SECTION

General Considerations. All experiments were performed under a dry nitrogen atmosphere using standard Schlenk techniques or an MBraun inert-gas glove box. Solvents were purified using a two-column solid-state purification system by the method of Grubbs[72] and transferred to the glovebox without exposure to air. $Me_2PhSiCl$, Et_3N, KH, 2,6-di-*tert*-butylphenol (HOAr), $[Bu_4N][I]$ (TBAI), and nBuLi were purchased from Alfa Aesar and used as received. $[Bu_4N][PF_6]$ ($TBAPF_6$), $[Et_3NH]Br$, and $NaBPh_4$ were purchased from Sigma Aldrich and recrystallized from THF before use. $H_2(NN^{TBS})$,[19] $H_2(NN^{TMS})$,[73] $H_2(NN^{DMP})$,[74] KCH_2Ph,[75] $LiNPh_2$,[76] $NaBAr^F$,[77] $TPABAr^F$ (tetraisopropylammonium tetrakis[3,5-bis(trifluoromethyl)phenyl]borate),[78] $UI_4(1,4\text{-dioxane})_2$,[79] $UI_4(Et_2O)_2$,[79] $(NN^{TBS})UI_2(THF)$,[79] $(NN^{TBS})U(CH_2Ph)_2$,[18] $(NN^{TMS})U(CH_2Ph)_2$,[80] and $(NN^{TBS})U(CH_2Ph)(OAr)$[37] were synthesized following previously published procedures. NMR solvents were obtained from Cambridge Isotope Laboratories, degassed, and stored over activated molecular sieves prior to use. ^1H and ^{13}C NMR spectra were recorded on Bruker300 or Bruker500 spectrometers at room temperature in C_6D_6 or $CDCl_3$. Chemical shifts are reported with respect to solvent residual peaks, 7.16 ppm (C_6D_6) or 7.26 ppm ($CDCl_3$). IR spectra were recorded on a JASCO FT-IR-420 spectrophotometer from 4000 to 400 cm^{-1} using a sealed liquid cell from International Crystals Laboratory with a 1 mm path length and KBr windows. Cyclic voltammetry measurements were conducted on a CH Instruments CHI630D potentiostat using a 2-mm platinum disk as the working electrode, 3-mm glassy carbon disk as the counter electrode, and 0.25-mm silver wire as the pseudo–reference electrode. CHN analyses were performed on an Exeter Analytical, Inc. CE-440 Elemental Analyzer.

Cyclic voltammetry. Most voltammetric measurements were conducted in tetrahydrofuran (THF) with $TPABAr^F$ as the supporting electrolyte. In some experiments, dichloromethane, α,α,α-trifluorotoluene (TFT), and diethyl ether (Et_2O) were used as solvents, while sodium tetrakis[3,5-bis(trifluoromethyl)phenyl]borate ($NaBAr^F$), tetrabutylammonium iodide (TBAI), and tetrabutylammonium hexafluorophosphate ($TBAPF_6$) served as electrolytes. ^1H NMR spectra of all complexes were acquired before and after each experiment in order to verify that no decomposition occurred in due course. When possible, electrochemical behavior of each compound was studied in various media to aid interpretation of data. A 2-mm platinum disk, 3-mm glassy carbon disk, and 0.25-mm silver wire were used as working, counter, and reference electrodes, respectively. Moreover, all redox potential values are mentioned with respect to that of ferrocene, which was added to the electrochemical cell at the end of each measurement.

DFT calculations. Computational studies were performed with ADF2012.01. For all atoms, except carbon and hydrogen, standard triple-ζ STA basis sets from the ADF database ZORA TZP were employed with the 1s-4f (U), 1s-3p (Fe), 1s-2p (Si, P), and 1s (N, C) electrons treated as frozen cores. The generalized gradient approximation (GGA) by Becke-Perdew was used together with the exchange and correlation corrections that are employed by default by the ADF2012.01 program suite. For NBO and Bader calculations, analysis was performed with full electron (no frozen cores) TZP basis sets and using the scalar ZORA approximation. Calculations were carried out using the scalar spin-orbit relativistic formalism. Mayer bond orders and atomic properties were calculated using the defaults implemented in the ADF2012.01 program suite. The optimized coordinates were used for further analysis with NBO 5.0[68] and Bader's Atoms In Molecules (AIM) methods, implemented in ADF.

Synthesis of $(NN^{DMP})UI_2(THF)$. A slurry of $[K_2(OEt_2)_2](NN^{DMP})$ (95 mg, 0.013 mmol, 0.9 equiv) in THF was added to a frozen THF solution of $UI_4(1,4\text{-dioxane})_2$ (137 mg, 0.015 mmol, 1 equiv). The reaction mixture was allowed to stir at room temperature for 1 h. It was then filtered through Celite. The filtrate was dried, the crude solid dissolved in toluene, then filtered through Celite and dried. Yield: 133 mg, 85%. $(NN^{DMP})UI_2(THF)$ is insoluble in hexanes, *n*-pentane, diethyl ether, slightly soluble in toluene, and completely soluble in THF and CH_2Cl_2. ^1H NMR (300 MHz, $CDCl_3$), δ (ppm): 55.7 (s, 12H, -Si(CH_3)$_2$), 51.9 (s, 4H, -Si(C_6H_5)), 13.6 (s, 4H, -Si(C_6H_5)), 11.1 (s, 2H, -Si(C_6H_5)), -19.2 (s, 4H, Cp*H*), -26.0 (s, 4H, -OC_4H_8), -39.4 (s, 4H, Cp*H*), -68.9 (s, 4H, -OC_4H_8). Elemental analysis for $C_{30}H_{38}FeI_2N_2OSi_2U$ (1046 g/mol): Calcd. 34.43% C, 3.66% H, 2.68% N; Found: 34.68% C, 3.61% H, 2.55% N.

Synthesis of $(NN^{DMP})U(CH_2Ph)_2$. A toluene slurry of KCH_2Ph (42.7 mg, 0.33 mmol, 2.1 equiv) was added to a cold toluene solution of $(NN^{DMP})UI_2(THF)$ (163.9 mg, 0.16 mmol, 1 equiv). After 75 min of stirring at room temperature, the solution was filtered through Celite and toluene was removed under reduced pressure. The product was extracted into hexanes. Yield: 128.6 mg, 89%. $(NN^{DMP})U(CH_2Ph)_2$ is soluble in all common organic solvents. Its stability in THF and halogenated solvents was not tested. ^1H NMR (300 MHz, C_6D_6), δ (ppm): 47.2 (s, 12H, -Si(CH_3)$_2$), 39.9 (s, 4H, -Si(C_6H_5)), 14.2 (s, 4H, -Si(C_6H_5)), 11.8 (s, 2H, -Si(C_6H_5)), -8.2 (s, 4H), -12.0 (s, 2H, -CH_2(C_6H_5)), -17.3 (s, 4H), -17.6 (s, 4H), -34.3 (s, 4H). Elemental analysis for $C_{40}H_{44}FeN_2Si_2U$ (903 g/mol): Calcd. 53.21% C, 4.91% H, 3.10% N; Found: 52.90% C, 4.83% H, 3.16% N.

Synthesis of $(NN^{TBS})UI(OAr)$. $(NN^{TBS})UI_2(THF)$ (165 mg, 0.16 mmol, 1 equiv) was dissolved in THF and solid KOAr (45 mg, 0.19 mmol, 1.5 equiv) was added. The solution became cloudy after 15 minutes of stirring at room temperature. The mixture was filtered through Celite after an additional 45 min and dried under reduced pressure. The product was extracted into hexanes, filtered through Celite, and dried. Yield: 155 mg, 94%. Dark-red rectangular crystals formed at -40 ºC after 1 h. Upon addition of one equivalent of KCH_2Ph, formation of $(NN^{TBS})U(OAr)(CH_2Ph)$ was detected by ^1H NMR

spectroscopy. Elemental analysis for $C_{36}H_{59}N_2Si_2OIFeU$ (1013 g/mol): Calcd. 42.69% C, 5.87% H, 2.77% N; Found: 43.15% C, 5.86% H, 2.72% N.

Synthesis of $(NN^{TBS})U(NPh_2)_2$. At room temperature, a THF solution of $LiNPh_2$ (14.2 mg, 0.07 mmol, 2 equiv) was slowly added to a stirring THF solution of $(NN^{TBS})UI_2(THF)$ (37.3 mg, 0.03 mmol, 1 equiv). The reaction mixture was allowed to stir at room temperature. After 30 min, the solvent was removed under reduced pressure to yield a red-brown oil. The product was extracted into hexanes, filtered, and dried. Finally, it was washed with cold *n*-pentane, and dried. Yield: 33.2 mg, 98%. $(NN^{TBS})U(NPh_2)_2$ is soluble in hexanes and *n*-pentane, but soluble in diethyl ether, toluene, and THF. ^{1}H NMR (300 MHz, C_6D_6), δ (ppm): 43.8 (s, 12H, -Si(CH_3)$_2$), 33.7 (s, 18H, -SiC(CH_3)$_3$), -3.1 (s, 4H), -5.2 (s, 8H), -18.7 (s, 4H), -28.7 (s, 8H), -37.3 (s, 4H). Elemental analysis for $C_{46}H_{58}FeN_4Si_2U$ (1017 g/mol): Calcd. 54.32% C, 5.75% H, 5.51% N; Found: 54.89% C, 5.72% H, 5.46% N.

ASSOCIATED CONTENT

Supporting Information. ^{1}H NMR, UV-Vis, NIR, and IR spectra, as well as details of the computational studies. This material is available free of charge via the Internet at http://pubs.acs.org.

AUTHOR INFORMATION

Corresponding Author

Email for P.L.D.: pld@chem.ucla.edu

ACKNOWLEDGMENT

The experimental and part of the computational work (SD, JVO, PLD) were supported by the U.S. Department of Energy, Office of Basic Energy Sciences, Heavy Element Chemistry program under Grant No. ER15984 (to PLD), and the Sloan Foundation. The rest of the computational work was supported by the U.S. Department of Energy, Office of Basic Energy Sciences, Heavy Element Chemistry program under Grant No. 2012LANLE372 (to ERB). JVO was supported by a LANL graduate student research fellowship during summer 2013.

REFERENCES

1. Gunanathan, C.; Milstein, D., *Acc. Chem. Res.* **2011,** *44* (8), 588.
2. Chirik, P. J.; Wieghardt, K., *Science* **2010,** *327* (5967), 794.
3. van der Vlugt, J. I., *Eur. J. Inorg. Chem.* **2012,** *2012* (3), 363.
4. Kaim, W., *Eur. J. Inorg. Chem.* **2012,** *2012* (3), 343.
5. Ray, K.; Petrenko, T.; Wieghardt, K.; Neese, F., *Dalton Trans.* **2007,** (16), 1552.
6. Diaconescu, P. L., *Comments Inorg. Chem.* **2010,** *31* (5-6), 196
7. Diaconescu, P. L., *Acc. Chem. Res.* **2010,** *43* (10), 1352.
8. Huang, W.; Dulong, F.; Wu, T.; Khan, S. I.; Miller, J. T.; Cantat, T.; Diaconescu, P. L., *Nat. Commun.* **2013,** *4*, 1448.
9. Green, A. G.; Kiesz, M. D.; Oria, J. V.; Elliott, A. G.; Buechler, A. K.; Hohenberger, J.; Meyer, K.; Zink, J. I.; Diaconescu, P. L., *Inorg. Chem.* **2013,** *52* (9), 5603.
10. Huang, W.; Diaconescu, P. L., *Chem. Commun.* **2012,** *48* (16), 2216
11. Huang, W.; Khan, S. I.; Diaconescu, P. L., *J. Am. Chem. Soc.* **2011,** *133* (24), 10410.
12. Elliott, A. G.; Green, A. G.; Diaconescu, P. L., *Dalton Trans.* **2012,** *41* (26), 7852
13. Broderick, E. M.; Guo, N.; Vogel, C. S.; Xu, C.; Sutter, J.; Miller, J. T.; Meyer, K.; Mehrkhodavandi, P.; Diaconescu, P. L., *J. Am. Chem. Soc.* **2011,** *133* (24), 9278.
14. Broderick, E. M.; Guo, N.; Wu, T.; Vogel, C. S.; Xu, C.; Sutter, J.; Miller, J. T.; Meyer, K.; Cantat, T.; Diaconescu, P. L., *Chem. Commun.* **2011,** *47*, 9897.
15. Huang, W.; Diaconescu, P. L., *Eur. J. Inorg. Chem.* **2013,** *2013* (22-23 (SI: Small-Molecule Activation by Reactive Metal Complexes)), 4090.
16. Broderick, E. M.; Thuy-Boun, P. S.; Guo, N.; Vogel, C. S.; Sutter, J.; Miller, J. T.; Meyer, K.; Diaconescu, P. L., *Inorg. Chem.* **2011,** *50* (7), 2870.
17. Monreal, M. J.; Khan, S. I.; Kiplinger, J. L.; Diaconescu, P. L., *Chem. Commun.* **2011,** *47*, 9119.
18. Monreal, M. J.; Diaconescu, P. L., *Organometallics* **2008,** *27*, 1702.
19. Monreal, M. J.; Carver, C. T.; Diaconescu, P. L., *Inorg. Chem.* **2007,** *46*, 7226.
20. Monreal, M. J.; Diaconescu, P. L., *J. Am. Chem. Soc.* **2010,** *132* (22), 7676.
21. Monreal, M. J.; Khan, S.; Diaconescu, P. L., *Angew. Chem. Int. Ed.* **2009,** *48* (44), 8352.
22. Duhović, S.; Monreal, M. J.; Diaconescu, P. L., *J. Organomet. Chem.* **2010,** *695* (25), 2822.
23. Duhović, S.; Monreal, M. J.; Diaconescu, P. L., *Inorg. Chem.* **2010,** *49* (15), 7165.
24. Bauer, J.; Braunschweig, H.; Dewhurst, R. D., *Chem. Rev.* **2012,** *112* (8), 4329.
25. Seyferth, D.; Hames, B. W.; Rucker, T. G.; Cowie, M.; Dickson, R. S., *Organometallics* **1983,** *2* (3), 472.
26. Akabori, S.; Kumagai, T.; Shirahige, T.; Sato, S.; Kawazoe, K.; Tamura, C.; Sato, M., *Organometallics* **1987,** *6* (10), 2105.
27. Shafir, A.; Arnold, J., *J. Am. Chem. Soc.* **2001,** *123* (37), 9212.
28. Carver, C. T.; Monreal, M. J.; Diaconescu, P. L., *Organometallics* **2008,** *27* (3), 363.
29. Monreal, M. J.; Carver, C. T.; Diaconescu, P. L., *Inorg. Chem.* **2007,** *46* (18), 7226.
30. Green, A. G.; Kiesz, M. D.; Oria, J. V.; Elliott, A. G.; Buechler, A. K.; Hohenberger, J.; Meyer, K.; Zink, J. I.; Diaconescu, P. L., *Inorg. Chem.* **2013,** *52* (9), 5603.
31. Ramos, A.; Otten, E.; Stephan, D. W., *J. Am. Chem. Soc.* **2009,** *131* (43), 15610.
32. Shafir, A.; Arnold, J., *J. Am. Chem. Soc.* **2001,** *123* (37), 9212.
33. Seyferth, D.; Hames, B. W.; Rucker, T. G.; Cowie, M.; Dickson, R. S., *Organometallics* **1983,** *2*, 472.
34. Mann, G.; Shelby, Q.; Roy, A. H.; Hartwig, J. F., *Organometallics* **2003,** *22* (13), 2775.
35. Metallinos, C.; Tremblay, D.; Barrett, F. B.; Taylor, N. J., *J. Organomet. Chem* **2006,** *691* (9), 2044.
36. Sato, M.; Suzuki, K.; Asano, H.; Sekino, M.; Kawata, Y.; Habata, Y.; Akabori, S., *J. Organomet. Chem.* **1994,** *470* (1-2), 263.
37. Broderick, E. M.; Gutzwiller, N. P.; Diaconescu, P. L., *Organometallics* **2010,** *29* (15), 3242.

38. Cordero, B.; Gomez, V.; Platero-Prats, A. E.; Reves, M.; Echeverria, J.; Cremades, E.; Barragan, F.; Alvarez, S., *Dalton Trans.* **2008,** (21), 2832.
39. Weydert, M.; Brennan, J. G.; Andersen, R. A.; Bergman, R. G., *Organometallics* **1995,** *14* (8), 3942.
40. Nicholson, R. S., *Anal. Chem.* **1965,** *37* (11), 1351.
41. Nicholson, R. S.; Shain, I., *Anal. Chem.* **1964,** *36* (4), 706.
42. Morris, D. E.; Da Re, R. E.; Jantunen, K. C.; Castro-Rodriguez, I.; Kiplinger, J. L., *Organometallics* **2004,** *23* (22), 5142.
43. Hoffman, R. V., *Organic Chemistry: An Intermediate Text*. Wiley: 2004.
44. Parsons, A. F., *An Introduction to Free Radical Chemistry*. Blackwell Science: 2000.
45. Bagnall, K. W.; Brown, D.; Colton, R., *J. Chem. Soc.* **1964**, 2527.
46. Bagnall, K. W.; Payne, G. F.; Alcock, N. W.; Flanders, D. J.; Brown, D., *J. Chem. Soc., Dalton Trans.* **1986,** (4), 783.
47. Moeller, T., *J. Chem. Ed.* **1970,** *47* (6), 417.
48. Denning, R. G., *J. Chem. Phys. A* **2007,** *111* (20), 4125.
49. Krupa, J. C., *J. Solid State Chem.* **2005,** *178* (2), 483.
50. Krupa, J. C., *J. Alloys Compd.* **1995,** *225* (1-2), 1.
51. Gutniak, S.; Taube, M., *Spectrochim. Acta* **1964,** *20* (10), 1627.
52. Edelstein, N. M., *J. Alloys Compd.* **1995,** *223* (2), 197.
53. Beattie, W. H.; Maier Ii, W. B.; Holland, R. F., *Spectrochim. Acta A* **1984,** *40* (10), 897.
54. Nugent, L. J.; Baybarz, R. D.; Burnett, J. L.; Ryan, J. L., *J. Inorg. Nucl. Chem.* **1971,** *33* (8), 2503.
55. Nugent, L. J.; Baybarz, R. D.; Burnett, J. L.; Ryan, J. L., *J. Chem. Phys.* **1973,** *77* (12), 1528.
56. Kirm, M.; Krupa, J. C.; Makhov, V. N.; Negodin, E.; Zimmerer, G.; Gesland, J. Y., *J. Lum.* **2003,** *104* (1-2), 85.
57. Cohen, D.; Carnall, W. T., *J. Chem. Phys.* **1960,** *64* (12), 1933.
58. Godbole, S. V.; Page, A. G.; Sangeeta; Sabharwal, S. C.; Gesland, J. Y.; Sastry, M. D., *J. Lum.* **2001,** *93* (3), 213.
59. Berg, J. M.; Sattelberger, A. P.; Morris, D. E.; Van der Sluys, W. G.; Fleig, P., *Inorg. Chem.* **1993,** *32* (5), 647.
60. Cho, Y. H.; Kim, T.-J.; Bae, S. E.; Park, Y. J.; Ahn, H. J.; Song, K., *Microchem. J.* **2010,** *96* (2), 344.
61. Krupa, J. C., *Inorg. Chim. Acta* **1987,** *139* (1-2), 223.
62. Kramer, J. A.; Hendrickson, D. N., *Inorg. Chem.* **1980,** *19* (11), 3330.
63. ADF2012.01; SCM http://www.scm.com: Theoretical Chemistry, Vrije Universiteit, Amsterdam, The Netherlands.
64. Velde, G. t.; Bickelhaupt, F. M.; Baerends, E. J.; Fonseca Guerra, C.; van Gisbergen, S. J. A.; Snijders, J. G.; Ziegler, T., *J. Comput. Chem.* **2001,** *22* (9), 931.
65. Fox, A. R.; Cummins, C. C., *J. Am. Chem. Soc.* **2009,** *131*, 5716.
66. Michalak, A.; DeKock, R. L.; Ziegler, T., *J. Phys. Chem. A* **2008,** *112* (31), 7256.
67. Glendening, E. D.; Badenhoop, J. K.; Reed, A. E.; Carpenter, J. E.; Bohmann, J. A.; Morales, C. M.; Weinhold, F., *NBO. Version 5.0*. Theoretical Chemistry Institute, University of Wisconsin: Madison, Wisconsin, USA, 2001.
68. Bader, R. F. W., *Atoms in Molecules - A Quantum Theory*. Oxford University Press: Oxford, 1990.
69. Rodríguez, J. I.; Bader, R. F. W.; Ayers, P. W.; Michel, C.; Götz, A. W.; Bo, C., *Chem. Phys. Lett.* **2009,** *472* (1-3), 149.
70. Fowe, E. P.; Therrien, B.; Suss-Fink, G.; Daul, C., *Inorg. Chem.* **2007,** *47* (1), 42.
71. Makal, A. M.; Plażuk, D.; Zakrzewski, J.; Misterkiewicz, B.; Woźniak, K., *Inorg. Chem.* **2010,** *49* (9), 4046.
72. Pangborn, A. B.; Giardello, M. A.; Grubbs, R. H.; Rosen, R. K.; Timmers, F. J., *Organometallics* **1996,** *15* (5), 1518.
73. Shafir, A.; Power, M. P.; Whitener, G. D.; Arnold, J., *Organometallics* **2001,** *20* (7), 1365.
74. Duhović, S.; Diaconescu, P. L., *Polyhedron* **2013,** *52* (SI: 100th Anniversary of the award of the 1913 Nobel prize in chemistry to Alfred Werner: A celebration), 377.
75. Bailey, P. J.; Coxall, R. A.; Dick, C. M.; Fabre, S.; Henderson, L. C.; Herber, C.; Liddle, S. T.; Lorono-Gonzalez, D.; Parkin, A.; Parsons, S., *Chem. Eur. J.* **2003,** *9* (19), 4820.
76. Sinha, A.; Schrock, R. R.; Müller, P.; Hoveyda, A. H., *Organometallics* **2006,** *25* (19), 4621.
77. Reger, D., Sodium Tetrakis(3,5-bis(trifluoromethyl)phenyl)borate, $Na[B(3,5\text{-}(CF_3)_2C_6H_3)_4]$. In *Inorganic Syntheses*, Shapley, J. R., Ed. Wiley-Interscience: 2004; Vol. 34, p 5.
78. Thomson, R. K.; Scott, B. L.; Morris, D. E.; Kiplinger, J. L., *C. R. Chim.* **2010,** *13* (6-7), 790.
79. Monreal, M. J.; Thomson, R. K.; Cantat, T.; Travia, N. E.; Scott, B. L.; Kiplinger, J. L., *Organometallics* **2011,** *30* (7), 2031.
80. Duhović, S.; Khan, S.; Diaconescu, P. L., *Chem. Commun.* **2010,** *46* (19), 3390.